SP Science Press

ARTICLE

Microstructure and Properties of 93W-4.6Ni-2.4Fe Prepared by Ball-Milling and Liquid Phase Sintering

Wang Zitong[1], Dong Di[2], Xiong Ning[2], Xu Jiawei[3], Dong Zhi[1], Ma Zongqing[1]

[1] School of Materials Science and Engineering, Tianjin University, Tianjin 300072, China; [2] ATTL Advanced Materials Co., Ltd, Beijing 100094, China; [3] Haitian Plastics Machinery Group Co., Ltd, Ningbo 315801, China

Abstract: In order to produce economical tungsten alloys with superior mechanical properties, 93W-4.6Ni-2.4Fe (wt%) tungsten heavy alloys were fabricated by ball milling and liquid phase sintering at a temperature range of 1450–1510 °C. The microstructure and the fracture modes of the specimens were examined. Results show that the specimens sintered at different temperatures display similar dual-phase microstructure and ductile fracture modes. With the increase in sintering temperature, the tungsten particle size also gradually grows. At the temperatures above 1480 °C, the relative density reaches above 99.0%. The optimal sintering temperature of the specimen with the best tensile strength (940 MPa) and elongation (32.6%) combination is determined to be 1480 °C. The excellent ductility of the specimen sintered at 1480 °C is associated with the network structure of γ phase, the uniform distribution of dimples and the synergistic effect of these two phases. The high strength of the specimen is attributed to the refined tungsten particle size and the spherical tungsten particles.

Key words: tungsten heavy alloy; ball-milling; liquid phase sintering; mechanical properties

Tungsten heavy alloys (WHAs) are employed in many areas like kinetic energy penetrators, crankshaft balance weights, precision tools for machining and optical precision instruments, due to the unique combination of high density, high strength, excellent plasticity and good corrosion resistance[1–3]. However, there still remain challenges in obtaining alloys with both high strength and high plasticity, especially when considering the cost of time and money.

The mechanical performance and the fracture behavior of WHA are determined mainly by componential and microstructural factors[4]. German et al[5] researched the performance of WHA with the tungsten content ranging from 90wt% to 97wt%. It is found that the ultimate tensile strength is insensitive to the tungsten content until it exceeds 97wt%. On the contrary, the elongation decreases with the continuous increase in tungsten content, and the decrease in ductility is quite rapid when the tungsten content exceeds 95wt% . Therefore, higher tungsten content will generally deteriorate the mechanical properties. Besides, fine powder (especially nano-sized powder) has higher sintering activity, thus making

it easier to achieve better densification in a short period of time. In addition to the raw material of WHA, the microstructural parameters of the alloy, such as the morphology of W particles, the volume fraction and distribution state of γ phase and the proportion of tungsten-tungsten interface, also have a significant impact on the alloy properties[6]. Contiguity is a measure of the W-W interfacial area fraction of the total grain boundaries, which is also a particularly important parameter to judge the properties of liquid phase sintered materials[7]. It is measured by the following equation:

$$C = \frac{2N_{\text{W-W}}}{2N_{\text{W-W}} + N_{\text{W-M}}} \tag{1}$$

where $N_{\text{W-W}}$ and $N_{\text{W-M}}$ are the numbers of W-W interfaces and W-γ phase interfaces[1], respectively. In addition, an excellent interface bonding between tungsten particles and matrix is essential to achieve better mechanical properties[8].

The microstructural characteristics mentioned above can be tailored through adjustment in processing conditions of WHA, such as sintering temperature, time, atmosphere and post-sintering thermomechanical treatments[9]. In fact, proper

manufacturing conditions are the prerequisite for obtaining high-performance tungsten heavy alloys[10]. Due to the high melting point and the high hardness of tungsten, powder metallurgy is generally selected to prepare WHA. The methods of alloy sintering include traditional liquid phase sintering (LPS), spark plasma sintering (SPS) and microwave sintering (MS). Hu et al[11] prepared 93W-5.6Ni-1.4Fe heavy alloys with similar liquid-phase sintered microstructure via SPS at solid-state sintering temperature and found that the ultimate tensile strength of the fabricated alloy is 1010 MPa due to fine grain strengthening. However, the ductility is only 5.5% because of the insufficient liquid phase formation and high contiguity. Liu et al[12] researched the mechanical properties and microstructure evolution of 93W-4.9Ni-2.1Fe (wt%) alloys via MS and found that with the increase in MS temperature, the distribution of tungsten grains and matrix phase becomes more homogeneous, and the W-matrix inter-facial bonding strength is enhanced. At the sintering tempe-rature of 1500 °C, the mechanical properties are significantly improved, and the ultimate tensile strength and the ductility are 1185.6 MPa and 16.4%, respectively. Sintering methods like SPS and MS can effectively suppress tungsten particle growth and improve the ultimate tensile strength of speci-mens, but the ductility is often less than 20%. On the contrary, conventional LPS has been widely used in industry[13–16] to acquire high-performance WHA with considerable strength and excellent ductility. The sintered WHA possesses a characteristic microstructure of near-spheroidal hard tungsten grains (20 – 60 μm), embedded in a ductile binder phase (matrix). During the LPS stage, the binder phase exists as a liquid phase, which promotes the rearrangement of tungsten particles and the migration of tungsten atoms[17]. On the one hand, the gap between tungsten particles is filled with liquid binder phase, and the capillary force and viscous flow of the liquid phase make the tungsten particles reposition and rearrange continuously. On the other hand, the edge and corner on the surface of small tungsten particles are prefer-entially dissolved, and the supersaturated tungsten atoms in the liquid binder phase re-precipitate on the surface of large particles. Therefore, liquid phase sintering is an easy way to obtain specimens with high density and uniform microstruc-ture, which is beneficial for obtaining high-performance specimens. With all things considered, LPS was selected in this work to prepare tungsten heavy alloys with excellent performance.

Attempts have been made in this work to prepare high-performance 93W-4.6Ni-2.4Fe alloys possessing better strength and plasticity by ball milling and LPS method. In order to figure out the optimum parameter of LPS, three different sintering temperatures including 1450, 1480 and 1510 °C were adopted and the relationship among sintering temperature, microstructure, mechanical property and fracture mechanism of the alloys was explored.

1 Experiment

In this study, nano-W powders (prepared by freeze drying method, explicitly explained in Ref.[18–19]) and commercial Ni and Fe powders (with a size of 2–5 μm and a purity of 99.99%) were used as raw materials. The content of tungsten element was determined to be 93wt% considering the comprehensive performance and the actual requirements. The ratio of nickel to iron was determined as 7:3 to avoid the formation of intermetallic phases[20]. Planet type ball-milling was used to gain the composite powders containing 93wt% W, 4.6wt% Ni and 2.4wt% Fe. Tungsten powder, nickel powder, iron powder and 304 stainless steel grinding balls (with the ball to powder mass ratio of 5:1 and big ball to small ball ratio of 1:4) were added in mass proportion to ball milling tanks, and then the tanks were tightened with a hex wrench. The entire process was operated in a glove box so that the tanks were filled with argon to protect powder from oxidation. The powders were milled at a speed of 200 r/min for 3 h. The ball-milled powders were then calcined in hydrogen atmosphere at 800 °C for 30 min to remove oxygen impurities. The ball-milled powder after annealing is shown in Fig.1. The average particle size of the powder was 0.30±0.16 μm.

After pressing in a mold with 25 mm in diameter under pressure of 10 MPa for 5 min, the powder compacts were sintered in hydrogen atmosphere at 1450, 1480 and 1510 °C for 90 min with the heating rate of 2 – 10 ° C/min. After sintering, the specimens were furnace cooled to room temperature.

The as-sintered specimens were prepared for subsequent microstructure and performance tests. Wire cutting was used to separate the specimens into cubes of 10 mm×10 mm×1.5 mm, which were eroded after grinding and polishing. The eroding solution consisting of 1 g $K_3[Fe(CN)_6]$, 1 g NaOH and 10 mL deionized water and the eroding time was 15 s. The crystal structure of composite powders and alloys was characterized by X-ray diffraction (XRD, D/MAX-2500) with Cu-Kα radiation. The scanning range of the diffraction angle 2θ was 30°−90° with a stepping size of 0.2° and a stepping time of 0.2 s. The microstructure of specimens was characte-rized by a field emission scanning electron microscope (SEM, JSM-7800F). Archimedes method was used to measure the actual density and to calculate the density of sintered specimens. The theoretical density of 93W-4.6Ni-2.4Fe alloy
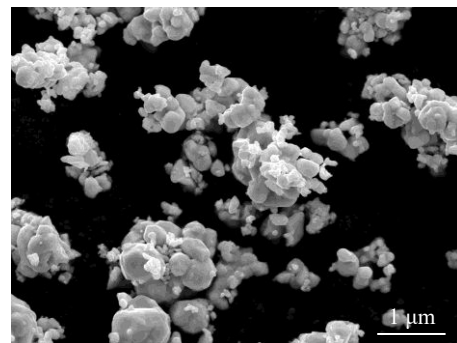

Fig.1 SEM image of ball-milled 93W-4.6Ni-2.4Fe powder after hydrogen annealing

is 17.76 g/cm^3[21]. Room temperature tensile tests were performed on an Instron 5869 material testing machine at a constant strain rate of 1×10^{-3} s^{-1}.

2 Results and Discussion

2.1 Phase composition and microstructure of 93W-4.6Ni-2.4Fe

The XRD patterns in Fig. 2 show that the dominant diffraction peak of both the original powder and the sintered specimens is bcc tungsten phase, while the relatively weak diffraction peak is γ (W, Ni, Fe) phase[22–26]. There are no diffraction peaks of other intermetallic compounds in XRD pattern of 93W-4.6Ni-2.4Fe powder, indicating the complete reduction of the powder.

Fig. 3 shows the SEM images of specimens sintered at different temperatures. In all three specimens, bcc tungsten particles, which are the bright region of images, are dispersed in the fcc Ni-Fe-W matrix, which is the dark region of images. According to the Fe-Ni phase diagram[27], the eutectic temperature of nickel and iron is 1440 °C at the mass ratio of 7∶3. Therefore, sintering at 1460 °C for 90 min can provide enough energy for γ phase to form and to flow adequately. Meanwhile, the tungsten grains undergo rapid separation and dispersion in a brief time span[28]. According to the Ostwald ripening mechanism, tungsten atoms dissolute and re-precipitate on coarser tungsten grains. It can be found in Fig.3 and Table 1 that with the increase in sintering temperature within the range of 1450–1510 °C, the growth of tungsten grains and the increase in density occur simultaneously. This is due to the presence of the liquid phase which accelerates densification[29]. At the sintering temperature of 1450 °C, although the tungsten particles exhibit a spherical morphology with an average size of 21.2±0.62 μm, binder phase is separated within several tungsten particles. The insufficient sintering is also reflected in the density of the specimen, which is only 94.8%±0.19%. Besides, microscale γ phase is found inside tungsten particles, which is attributed to the blending of W and Ni/Fe powder during the ball milling process. When the sintering temperature increases to 1480 °C, the size of tungsten particles increases to 33.7±1.1 μm and the

density of the specimen also increases to above 99.0%. At this temperature, the binder phase gradually infiltrates between W particles, leading to the formation of a two-phase structure with a network of ductile phases separating hard tungsten particles. Furthermore, a reduction in contiguity from 0.51± 0.06 to 0.41±0.09 and an increment of γ phase content from 9.0vol%±0.16vol% to 16.9vol%±0.07vol% are found compared with those of specimen sintered at 1450 °C. As the sintering temperature further increases from 1480 °C to 1510 °C, the size of tungsten particles slightly increases to 34.7±1.8 μm and the γ phase content reduces to 14.1vol%±0.15vol%. The slight increase in particle size and the change of γ phase volume fraction result in more contact among large-sized tungsten particles, thereby raising the contiguity to 0.45±0.08[7,21].

2.2 Mechanical properties and fracture modes of 93W-4.6Ni-2.4Fe

The engineering stress-strain curves of the specimens sintered at different temperatures are presented in Fig.4a, and the specific values of tensile strength and elongation of specimens sintered at different temperatures are presented in Table 2. The specimens sintered at different temperatures exhibit similar ductile fracture modes. It can be easily found that the specimen sintered at 1450 °C has the highest ultimate tensile strength of 954 MPa. The ultimate tensile strength of the specimen sintered at 1480 °C is decreased by 14 MPa, but the total elongation significantly increases to 32.6%. It is also found that the specimen sintered at 1510 °C possesses the lowest ultimate tensile strength of 843 MPa and the lowest elongation of 10.0%. Based on the above data, the specimen prepared by ball milling followed by sintering at 1480 °C achieves the best combination of strength and ductility. Fig.4b compares the mechanical performance of specimens in this work and other works with similar tungsten composition and powder preparation method[4,11,12,14,30–34]. As can be seen from Fig.4b, WHA fabricated by LPS without heat treatment (HT, in the green ellipse) has relatively low elongation of less than 25%. WHA fabricated by LPS with HT (in the orange ellipse) or by other sintering methods, such as MS and two-step sintering (TS), exhibits outstanding tensile strength of over 900 MPa and high elongation between 25% and 30%.

Compared with the mechanical performance of 89-93W specimens in other literatures, the specimen in this work presents a comparative ultimate tensile strength and an excellent elongation, especially when compared with those fabricated by LPS without HT.

The tensile fracture of the specimens sintered at different temperatures is shown in Fig.5. In WHA systems, the ductile matrix serves as a binder for the brittle tungsten grains and releases stress as deformation takes place during room temperature tensile test. General fracture in tungsten heavy alloys is composed of four modes including W-W interparticle fracture (WF), W cleavage (WC), W-matrix γ phase interfacial separation (W/γD) and matrix γ phase rupture (γR). WHA is a two-phase alloy that contains W-W interfaces and W-γ
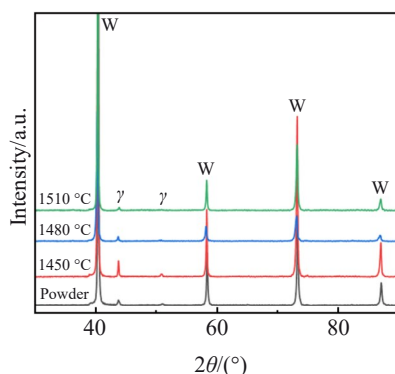

Fig.2　XRD patterns of 93W-4.6Ni-2.4Fe powder and specimens sintered at 1450 °C, 1480 °C, and 1510 °C for 1.5 h
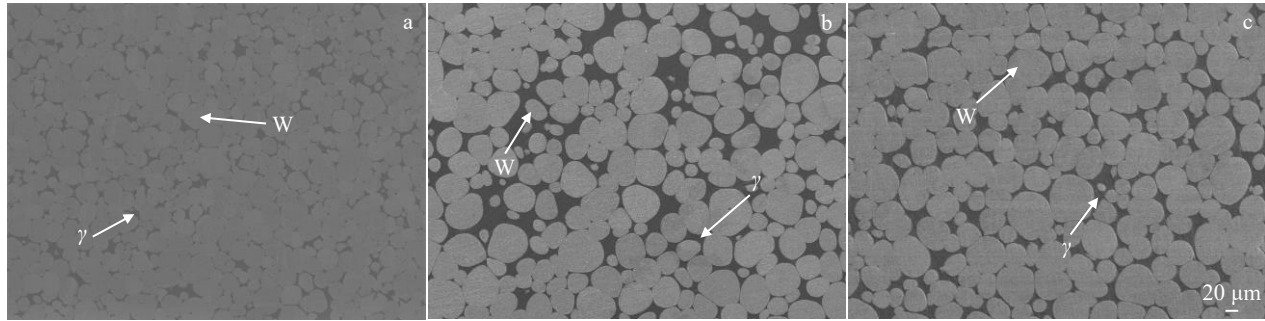
Fig.3   SEM images of 93W-4.6Ni-2.4Fe specimens sintered at 1450 °C (a), 1480 °C (b), and 1510 °C (c) for 1.5 h

Table 1   Physical properties of 93W-4.6Ni-2.4Fe specimens sintered at different temperatures

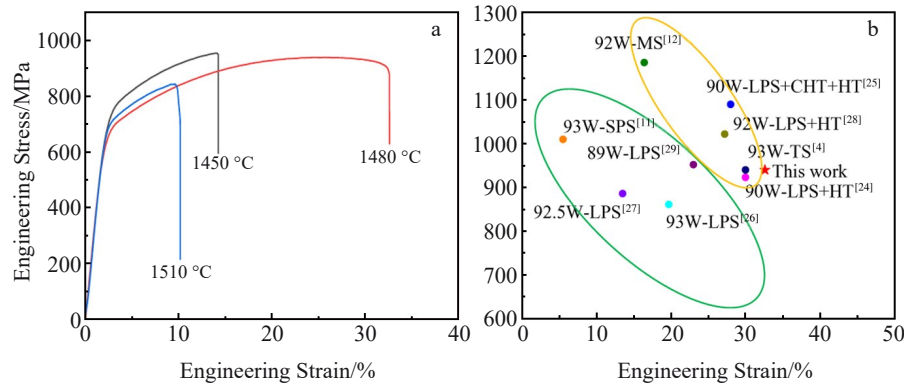| Sintering temperature/°C	Size of tungsten particle/μm	Relative density/%	Contiguity	γ phase content/vol%
1450	21.2±0.62	94.8±0.19	0.51±0.06	9.0±0.16
1480	33.7±1.1	99.1±0.06	0.41±0.09	16.9±0.07
1510	34.7±1.8	99.7±0.22	0.45±0.08	14.1±0.15

Fig.4   Tensile stress-strain curves of 93W-4.6Ni-2.4Fe specimens sintered at different temperatures (a) and comparison between the mechanical performance of WHA with similar tungsten content in literatures and in this work (b)

Table 2   Mechanical properties of 93W-4.6Ni-2.4Fe specimens sintered at different temperatures

Sintering temperature/°C	Ultimate tensile strength/MPa	Elongation/%
1450	954	14.2
1480	940	32.6
1510	843	10.0

interfaces. The proportion and bonding strength of these two interfaces determine the quasi-static mechanical properties of the alloy. When the proportion of W-W interfaces increases, which perform as crack, the sintering is not sufficient, and alloys tend to fracture prematurely. However, when the sintering process is complete and W-γ interfaces undergo sufficient diffusion, the uniform distribution of network γ phase and the improvement in interface strength can contribute to stress dispersion and fracture delay. It can be seen in Fig.5a and 5b that the fracture surface mainly presents

a rock sugar shape like intergranular fracture morphology. The relatively high contiguity of the specimen sintered at 1450 °C leads to fracture of a large number of W-W interparticles, which is the main reason why the specimen obtains the low elongation of only 14.2%. The best ultimate tensile strength of the specimen acquired at specific sintering temperature is due to the small tungsten particle size, which can be explained by fine grain strengthening. With the increase in sintering temperature, the W cleavage tendency ascends first and then descends, so does the matrix γ phase rupture. There is a large amount of W-matrix γ phase interfacial separation in the specimen sintered at 1480 °C due to the decrease of W-W interfaces, as shown in Fig. 5c. Specially, there are obvious ripple like slip lines on the intergranular fracture surface of W particles in Fig. 5d, representing the high bonding strength of tungsten particles and the matrix phase, which is related to the reduction in the interparticle fracture and the increase in engineering strain. Compared with γ dimples in specimen sintered at 1450 °C in Fig. 5b, the dimples in Fig. 5d are
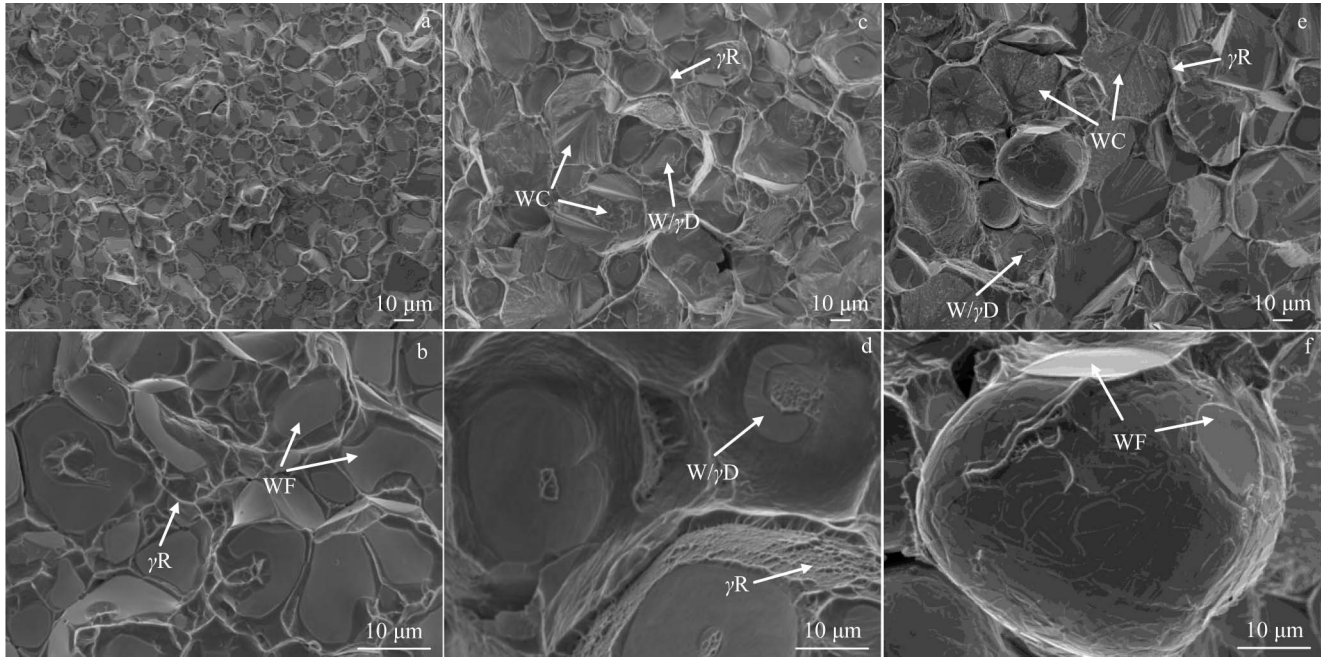
Fig.5　Tensile fracture morphologies of 93W-4.6Ni-2.4Fe specimens sintered at (a–b) 1450 °C, (c–d) 1480 °C, and (e–f) 1510 °C for 1.5 h

significantly denser and the dimple size is finer, with a greater degree of tearing, which is consistent with the elongation data of the two specimens. There are not only W cleavages and matrix *γ* phase ruptures in Fig. 5e and 5f, but also some tungsten particles with spherical shape and weak bonding to interfaces. In this case, W-W interparticle fracture dominates the initiation and propagation of cracks, leading to early fracture of the specimen.

Table 3 shows the relative percentage of four fracture modes in specimens sintered at different temperatures, which were stated by linear intercept method[35]. At the sintering temperature of 1450 °C, the proportion of W-W interparticle fracture and matrix *γ* phase rupture reaches to above 90%, while the proportion of W cleavage is only 2.5% and W-matrix *γ* phase interfacial separation is 5.1%. Because the fracture process of WHA is initiated via local failure at W-W interfaces[36], the high proportion of W-W interfacial fracture (37.8%) is detrimental to the specimen performance. Matrix *γ* phase rupture and W cleavage dominate the tensile fracture at the sintering temperatures of 1480 and 1510 °C. With the ascendance of sintering temperature from 1450 °C to 1480 °C, the proportion of W-W interparticle fracture is significantly reduced from 37.8% to 13.0%, while the proportion of W cleavage is dramatically advanced from 2.5% to 31.7%. The proportion of matrix *γ* phase rupture and W-matrix *γ* phase interfacial separation is 44.4% and 10.9%, respectively. The

high proportion of W-matrix *γ* phase interfacial separation is attributed to the fine W-*γ* interface strength and the low contiguity, compared with the other two sintered specimens. On the contrary, the insufficient sintering at 1450 °C results in insufficient formation of *γ* phase and poor interface connectivity between tungsten particles and *γ* phase, whereas the excessive growth of tungsten particles at 1510 °C leads to the increase in W-W connecting, causing the increase in contiguity and the decrease in W-matrix *γ* phase interfacial separation proportion for both of the sintering temperatures. In addition, W-W interparticle fracture has the lowest fraction (7.6%) among the three specimens and W cleavage has the highest fraction (48.1%), because the specimen sintered at 1510 °C processes the largest tungsten particle size.

Fig. 6 shows the longitudinal section near the tensile fracture of the specimen sintered at different temperatures. It can be seen from Fig. 6a that once cracks initiate, they can extend either along the tungsten particle interfaces or pass though particles. When sintering temperature increases to 1480 °C, the crack morphology changes significantly. Cracks tend to extend and propagate within the tungsten particles, which can be separated and interrupted by the *γ* network. The synergy of hard tungsten and ductile matrix enables the achievement of high elongation and comparable strength. Fig.6d shows a local magnification of the cracks in Fig.6c at the sintering temperature of 1510 °C, where the intragranular

Table 3　Percentage of four tensile fracture features of 93W-4.6Ni-2.4Fe specimens sintered at different temperatures

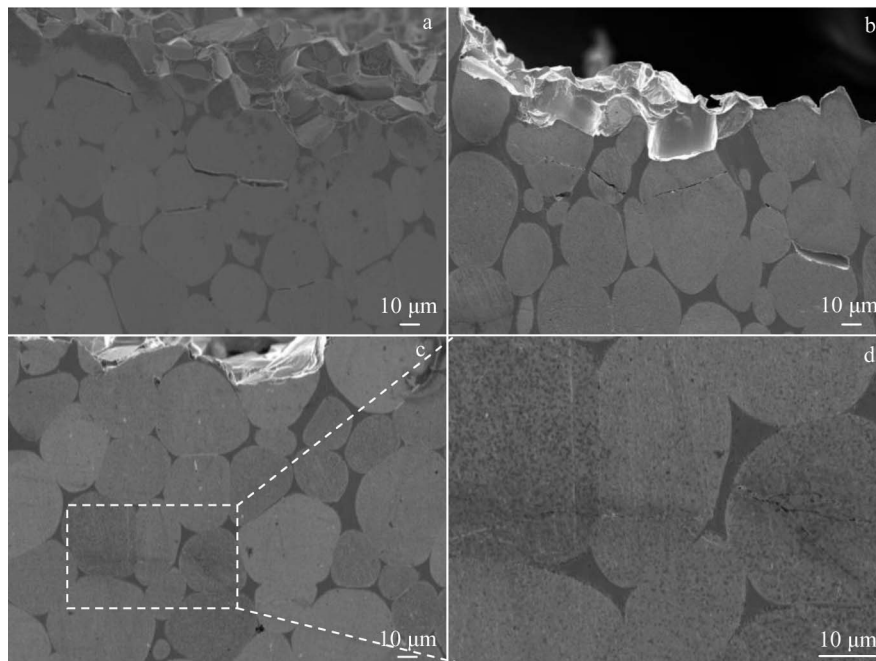| Sintering temperature/°C	W-W interfacial fracture/%	Matrix *γ* phase rupture/%	W cleavage/%	W-matrix *γ* phase interfacial separation/%
1450	37.8	54.6	2.5	5.1
1480	13.0	44.4	31.7	10.9
1510	7.6	38.6	48.1	5.7

Fig.6   SEM images of longitudinal section near the tensile fracture edge of 93W-4.6Ni-2.4Fe tensile specimen sintered at 1450 ° C (a), 1480 °C (b), and 1510 °C (c–d) for 1.5 h

cracks are reduced in size and tend to merge with each other due to the grain growth.

3 Conclusions

1) Focused on 93W-4.6Nic-2.4Fe alloys prepared by ball milling and LPS, the microstructure and mechanical properties of specimens sintered at different temperatures are studied. With the increase in sintering temperature, the tungsten particle size and the relative density of the specimen increase synchronously.

2) Specimen sintered at 1480 ° C for 1.5 h possesses high relative density (99.1%±0.06%) and the best combination of tensile strength (940 MPa) and elongation (32.6%).

3) The high ductility of the specimen is attributed to the network structure of γ phase, the uniform distribution of dimples and the synergistic effect of two phases. The high strength of the specimen is attributed to the refined tungsten particle size and the spherical tungsten particles.

References

1   Senthilnathan N, Annamalai A R, Venkatachalam G. *Transactions of the Indian Institute of Metals*[J], 2017, 70(5): 1161

2   Gnanasambandam P, Kumar A R, Nandy K T. *Defense Science Journal*[J], 2021, 71(4): 564

3   Shao Y, Yu W, Wu J *et al. Materials*[J], 2022, 15(22): 8035

4   Ryu H J, Hong S H. *Materials Science and Engineering A*[J], 2003, 363(1–2): 179

5   German R M, Bourguignon L L, Rabin B H. *Journal of the Minerals, Metals & Materials Society*[J], 1985, 37: 36

6   Lee K H, Cha S I, Ryu H J *et al. Materials Science and Engineering A*[J], 2007, 458(1–2): 323

7   German R M. *Metallurgical Transactions A*[J], 1985, 16: 1247

8   Islam S H, Qu X, He X. *Powder Metallurgy*[J], 2007, 50: 11

9   Dinçer O, Pehlivanoğlu M K, Çalişkan N K *et al. International Journal of Refractory Metals and Hard Materials*[J], 2015, 50: 106

10   Manikandan R, Annamalai A R. *Processes*[J], 2022, 10(11): 2352

11   Hu K, Han C, Khanlari K *et al. Advanced Engineering Materials*[J], 2023, 25(5): 2200615

12   Liu W S, Ma Y Z, Zhang J J. *International Journal of Refractory Metals and Hard Materials*[J], 2012, 35: 138

13   Skoczylas P, Gulbinowicz Z, Goroch O *et al. Problemy Mechatroniki*[J], 2019, 10: 23

14   Skoczylas P, Kaczorowski M. *Materials*[J], 2022, 15(24): 9064

15   Kunčická L, Kocich R, Klečková Z. *Materials*[J], 2022, 13(10): 2338

16   Li Z, Zhang H, Zhang G *et al. Metallurgical and Materials Transactions A*[J], 2022, 53: 1085

17   Cheng Xingwang, Wang Fuchi, Li Shukui *et al. Rare Metal Materials and Engineering*[J], 2006, 35(11): 1761 (in Chinese)

18   Hu W, Dong Z, Yu L *et al. Journal of Materials Science & Technology*[J], 2020, 36: 84

19   Hu W, Dong Z, Wang H *et al. International Journal of Refractory Metals and Hard Materials*[J], 2021, 95: 105453

20   German R M, Hanafee J E, DiGiallonardo S L. *Metallurgical Transactions A*[J], 1984, 15:121

21   Hu Z, Liu Y, Wu J *et al. Additive Manufacturing*[J], 2021, 46: 102216

22   Xue Sa, Wang Qingxiang, Liang Shujin *et al. Rare Metal*

Materials and Engineering[J], 2023, 52(5): 1943 (in Chinese)

23 Bose A, Reidy P J, Tuncer N *et al. International Journal of Refractory Metals and Hard Materials*[J], 2023, 110: 106021

24 Li Z B, Zhang G H, Chou K C. *Journal of Alloys and Compounds*[J], 2023, 969: 172361

25 Su X W, He Z, Yin T *et al. Materials Science and Engineering A*[J], 2023, 879: 145298

26 Alam M E, Odette G R. *Nuclear Materials and Energy*[J], 2023, 36: 101467

27 Swartzendruber L J, Itkin V P, Alcock C B. *Journal of Phase Equilibria*[J], 1991, 12: 288

28 Eliasson A, Ekbom L, Fredriksson H. *Powder Metallurgy*[J], 2008, 51(4): 343

29 Bose A, German R M. *Metallurgical Transactions A*[J],1988, 19: 3100

30 Kiran U R, Panchal A, Kamal S S K *et al. Defense Science Journal*[J], 2023, 73(2): 241

31 German R M, Bose A. *Metallurgical Transactions A*[J], 1990, 21: 1325

32 Li Z, Wang Y, Zhang H *et al. Materials Science and Engineering A*[J], 2021, 825: 141870

33 Alam M E, Odette G R. *Acta Materialia*[J], 2020, 186: 324

34 Kiran U R, Panchal A, Kumar M P *et al. Journal of Alloys and Compounds*[J], 2017, 709: 609

35 Hu K, Li X, Liu B *et al. Advanced Engineering Materials*[J], 2021, 23(4): 2001283

36 Clayton J D. *Theoretical and Applied Fracture Mechanics*[J], 2006, 45(3): 163

球磨和液相烧结制备 W-Ni-Fe 合金的组织和力学性能

王姿瞳[1]，董　帝[2]，熊　宁[2]，徐嘉伟[3]，董　智[1]，马宗青[1]

(1. 天津大学 材料科学与工程学院，天津　300072)

(2. 安泰天龙钨钼科技有限公司，北京　100094)

(3. 海天塑机集团有限公司，浙江　宁波　315801)

摘　要：为了制备出优异、经济友好的钨重合金，在1450~1510 ℃的烧结温度范围内，通过球磨和液相烧结制备了93W-4.6Ni-2.4Fe（质量分数）合金。进一步研究了试样的微观结构和断裂模式。结果表明，在不同烧结温度下，烧结的试样表现出相似的两相显微结构和韧性断裂模式。随着烧结温度的升高，钨颗粒尺寸也逐渐增大。当烧结温度达到或超过1480 ℃时，合金相对密度达到99.0%以上。1480 ℃烧结时可获得具有最佳抗拉伸强度（940 MPa）和延伸率（32.6%）组合的试样。在1480 ℃下烧结的试样具有优异的延展性，这与γ相的网络结构、韧窝的均匀分布以及两相的协同作用有关。试样的高强度归因于细化的钨颗粒尺寸和球形的钨颗粒。

关键词：钨重合金；球磨；液相烧结；力学性能